Environmental Science & Technology

ARTICLE

pubs.acs.org/est

Effects of Humic Substances on Precipitation and Aggregation of Zinc Sulfide Nanoparticles

Amrika Deonarine,[‡] Boris L.T. Lau,[§,‡] George R. Aiken,[⊥] Joseph N. Ryan,[∥] and Heileen Hsu-Kim*[,‡]

[‡]Department of Civil and Environmental Engineering, Duke University, Box 90287, Durham, North Carolina 27708, United States

[⊥]U.S. Geological Survey, 3215 Marine Street, Boulder, Colorado 80303, United States

[∥]Department of Civil, Environmental and Architectural Engineering, University of Colorado, Boulder, Colorado 80309, United States

Supporting Information

ABSTRACT: Nanoparticulate metal sulfides such as ZnS can influence the transport and bioavailability of pollutant metals in anaerobic environments. The aim of this work was to investigate how the composition of dissolved natural organic matter (NOM) influences the stability of zinc sulfide nanoparticles as they nucleate and aggregate in water with dissolved NOM. We compared NOM fractions that were isolated from several surface waters and represented a range of characteristics including molecular weight, type of carbon, and ligand density. Dynamic light scattering was employed to monitor the growth and aggregation of Zn−S−NOM nanoparticles in supersaturated solutions containing dissolved aquatic humic substances. The NOM was observed to reduce particle growth rates, depending on solution variables such as type and concentration of NOM, monovalent electrolyte concentration, and pH. The rates of growth increased with increasing ionic strength, indicating that observed growth rates primarily represented aggregation of charged Zn−S−NOM particles. Furthermore, the observed rates decreased with increasing molecular weight and aromatic content of the NOM fractions, while carboxylate and reduced sulfur content had little effect. Differences between NOM were likely due to properties that increased electrosteric hindrances for aggregation. Overall, results of this study suggest that the composition and source of NOM are key factors that contribute to the stabilization and persistence of zinc sulfide nanoparticles in the aquatic environment.

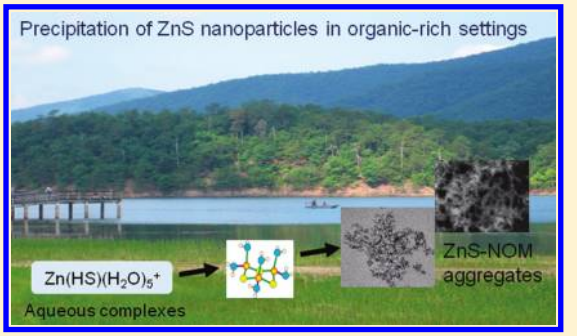

INTRODUCTION

The precipitation of metal sulfide minerals in the environment is traditionally viewed as a process that reduces the solubility and toxicity of contaminant metals such as Zn, Hg, Ag, and others.[1] Nanoclusters or nanocrystals of metal sulfides, however, are potentially mobile in the aquatic environment and can exhibit solubility properties that differ from those of larger materials of similar composition.[2] Nanoparticles would be expected under conditions of supersaturation, as they are the first formation products of a precipitation process. Nanoparticles of metal sulfides have been found in numerous settings, including anaerobic soil and sediments, biofilms of sulfate-reducing bacteria, wastewater effluent and biosolids, and other sulfidic environments.[3−8] ZnS and other metal sulfide particles tend to attach to themselves with high efficiency, due to high surface energies and isoelectric points near neutral pH.[9−11] However, metal sulfide nanoparticles also tend to exist in organic-rich waters where dissolved natural organic matter (NOM) can interfere with cluster formation and aggregation processes.

NOM is known to influence the aggregation rate of particles by adsorbing to the surface of particles and inducing electrostatic and electrosteric repulsive forces that alter aggregation kinetics.[12−14] Few studies, however, have considered how the composition of NOM contributes to such interactions. Humic substances vary widely according to their origin, and their composition is influenced by factors such as water chemistry, climate, and carbon source. Thus, they are not necessarily consistent in their manner of interaction with metal sulfide particle surfaces and subsequent surface reactivity. Previous work has indicated that NOM-induced dissolution rates of cinnabar (HgS) correlated to specific NOM components such as aromatic carbon content,[15,16] possibly due to redox-active moieties (e.g., quinones). Hydrophobic acid fractions of NOM (e.g., humic and fulvic acids) were found to decrease precipitation rates of HgS particles,[17] presumably by coating nanoparticles of HgS that remained stable in suspension.[18] Moreover, for NOM and high molecular weight polyelectrolyte surfactants, the conformation of the sorbed layer is critical for controlling electrosteric hindrances for aggregation.[12,13,19]

Humic substances also contain metal-binding functional groups that influence precipitation kinetics by forming dissolved complexes with metals and lowering the mineral saturation index,

Special Issue: Nanoscale Metal-Organic Matter Interaction

Received: August 30, 2010
Accepted: January 11, 2011
Revised: January 7, 2011
Published: February 03, 2011

Table 1. Aquatic Humic Substances for Zn−S−NOM Precipitation Studies (NOM Materials from the International Humic Substances Society (IHSS) Are Noted)

source	abbreviation	organic C source	site description
Suwannee River humic and fulvic acids	SRH, SRF	terrestrial	black water river draining the Okeefenokee Swamp at Fargo, GA (IHSS standard)
Ogeechee River humic and fulvic acids	OgRH, OgRF	terrestrial	piedmont region of eastern GA
Ohio River humic and fulvic acids	OhRH, OhRF	terrestrial	sampled at Cincinnati, Ohio
Missouri River fulvic acid	MRF	terrestrial	sampled at Sioux City, Iowa
Pacific Ocean fulvic acid	POF	autochtonous (marine)	sample collected from 100 m depth, 170 km southwest of Honolulu, Hawaii
Pony Lake fulvic acid	PLF	autochthonous (microbe)	saline, eutrophic lake in Antarctica (IHSS reference)

the driving force for precipitation. Furthermore, ligands can stabilize or destabilize particle suspensions by specifically sorbing to particles' surfaces.[10,11,17] Our previous research has shown that low molecular weight organic acids with thiol (R-SH) functional groups are more effective than hydroxyl-containing analogues for adsorbing to the surface of metal sulfide nanoparticles and slowing aggregation rates.[11,18,20] Specificity of the thiol functional group stems from relatively higher binding constants for Zn, Hg, and other soft-sphere metals.

Reduced sulfur functional groups within NOM molecules are considered the strongest binding ligands for soft-sphere metals. They range in concentrations from 0.01 to 0.3 μmol S per mg C in aquatic humic substances.[16,21] NOM is an important portion of the total thiol pool that is typically near 0.001 to 1 μM in surface waters[22,23] and up to 100 μM in sediment porewater.[24,25] Oxygen- and nitrogen-containing functional groups associated with NOM are typically weaker ligands, yet more abundant than thiols.

In this study, we sought to determine how NOM influences the precipitation and aggregation of zinc sulfide nanoparticles and to identify specific properties of NOM that contribute to the stabilization of nanoparticles. We utilized humic and fulvic acids that were obtained from several different aquatic sources. Dynamic light scattering was used to monitor hydrodynamic diameter as the ZnS nanoparticles precipitated and aggregated in solutions with the humic substances. The presence of NOM, for the most part, decreased observed growth rates. Differences in rates were observed as a function of solute composition, NOM type, and NOM composition.

EXPERIMENTAL SECTION

Materials. All chemicals used in this study were ACS reagent grade. Ultrapure water (Barnstead Nanopure) was used to prepare all stocks. All glassware was cleaned by overnight soak in soap, overnight soak in 1 N HCl, and then three rinses with ultrapure water. Zn(II) stocks were prepared by dissolving $Zn(NO_3)_2$ in 0.1 N HNO_3. Sulfide stocks were prepared daily by dissolving $Na_2S\cdot 9H_2O$ crystals (rinsed and dried prior to weighing) in water purged with ultrahigh purity N_2.

Nine different NOM isolates obtained from surface water environments (Table 1) were selected to represent a wide range in composition. Suwannee River humic (2S101H) and fulvic (1S101F) acids and Pony Lake fulvic acid (1R109F) were obtained from the International Humic Substances Society (IHSS). Humic and fulvic acids from several other surface waters (outlined in Table 1) were extracted using standard methods.[26] NOM fractions from Pony Lake and the Pacific Ocean are considered endmembers for authochthonous carbon in surface waters whereas the other source waters contained NOM derived mainly from terrestrial environments.

All of these isolates have been characterized and described elsewhere (see Supporting Information Table S1) for their composition including major element content, carbon composition by ^{13}C nuclear magnetic resonance spectroscopy, molecular weight by size exclusion chromatography,[27,28] and reduced sulfur content by sulfur X-ray absorption near-edge spectroscopy.[29] For each NOM isolate, the specific ultraviolet absorbance at 280 nm ($SUVA_{280}$) was quantified based on the method described by Weishaar et al.[30]

NOM stocks were prepared in ultrapure water, adjusted to pH 6.0 using NaOH and HCl as needed, and filtered (0.2 μm pore size). Dissolved organic carbon (DOC) concentrations in the filtered stocks were quantified using combustion catalytic oxidation/infrared spectroscopy (Shimadzu). The measured DOC concentrations were used to estimate NOM content in the Zn−S−NOM samples.

Preparation of Zn−S−NOM Samples. Experimental solutions consisted of dissolved $NaNO_3$ (from 0.01 to 0.1 M) and 4 mM sodium 4-(2-hydroxyethyl) piperazine-1-ethanesulfonate (HEPES) buffered to pH 7.5. An aliquot of the NOM stock was added to this filtered (<0.2 μm) buffer solution, followed by sequential addition of Zn (5 μM) and then sulfide (5 μM), added within 5 min. $NaNO_3$ concentration as well as NOM type and concentration were varied to determine their effect on precipitation and particle growth rates. All experimental solutions were prepared in a HEPA-filtered laminar flow workstation under oxic conditions. With these conditions (neutral pH and equimolar Zn:S), sulfide did not oxidize appreciably over two days.[20]

A selection of precipitation experiments was performed in bicarbonate and sodium 3-(*N*-morpholino)propanesulfonic acid (MOPS) buffers and produced results similar to those of experiments with HEPES (SI Figure S1). Experiments with a phosphate buffer were not reproducible. HEPES buffer was chosen for all ZnS solutions to maintain consistency among experiments.

ZnS Particle Growth Kinetics. Hydrodynamic diameter of particles was monitored over time at 25 °C using dynamic light scattering (DLS) (Malvern Zetasizer NS) of the incident light (λ = 663 nm) at 173°. After preparation of the experimental sample, an aliquot was immediately dispensed into a polycarbonate cuvette and placed in the instrument sample holder. Intensity-weighted diameter was calculated from twenty consecutive 10 s measurements. In solutions containing the buffer and NOM (from 1 to 5 mg C/L), detector count rates were 50−60 kilocounts per second (kcps), a rate that is above rates for water alone (30 kcps). In both cases data quality was not sufficient for size estimation. Because our Zn−S−NOM samples consisted of polydisperse suspensions, size measurements were accepted only for samples that demonstrated light scattering rates greater than 70 kcps (for the same attenuation and detector settings), a threshold that was observed only when both Zn and S were added to NOM solutions.

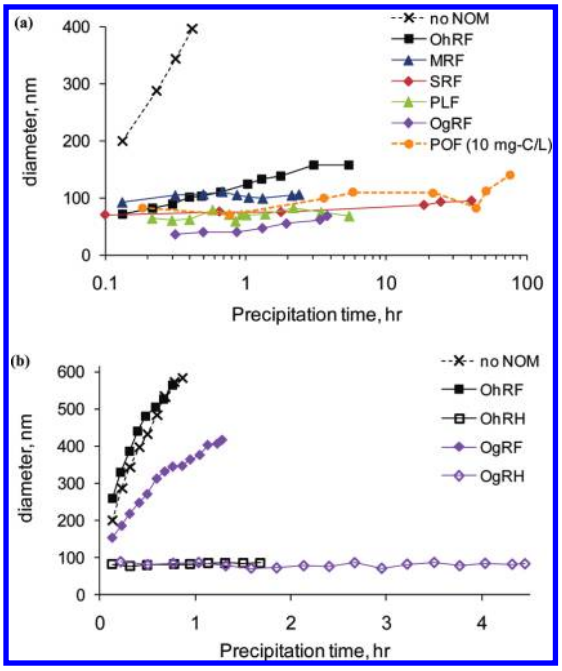

Figure 1. Hydrodynamic diameter of particles precipitating in solutions containing 5 μM $ZnNO_3$, 5 μM Na_2S, and dissolved NOM: (a) stabilization of nanoparticles by fulvic acids (5 mg-C/L) for hours to days; (b) comparison of fulvic and humic acid fractions in Zn−S−NOM mixtures containing 1 mg C/L. All samples contained 0.1 M $NaNO_3$ and 4 mM HEPES buffered to pH 7.5. Sample labels for NOM fractions: Ohio River fulvic and humic (OhRF and OhRH); Ogeechee River fulvic and humic (OgRF and OgRH); and fulvic acids from the Missouri River (MRF), Suwannee River (SRF), Pony Lake (PLF), and Pacific Ocean (POF).

Nucleation, precipitative growth, and aggregation of particles occurred simultaneously in the samples, resulting in polydisperse size distributions of aggregated nanoparticles. The hydrodynamic diameters reported in this study were based on light-intensity weighted measurements, which can bias toward larger particles (i.e., aggregates instead of monomers) in a polydisperse suspension. Moreover, sufficient scattering count rates for DLS are highly dependent on particle size and concentration. For example, the DLS instrumentation manufacturer recommends sample concentration for small particles (<10 nm) to be greater than 500 mg/L, a concentration much greater than that of our samples. Such limitations probably prevented adequate scattering from Zn−S−NOM monomer subunits, which were smaller than 10 nm (SI Figures S2 and S3). With this potential bias and the results we obtained (diameters greater than 50 nm), we interpreted the time-resolved DLS data (e.g., Figure 1) to reflect aggregation processes rather than nucleation of subunits and further growth of those subunits. Furthermore, the observed growth rates depended on the number of particles in suspension and particle−particle interactions during aggregation. Therefore, the DLS data were used for comparison of growth rates between mixtures rather than quantitative identification of particle size.

Linear regressions were performed between the NOM parameters (Table S1) and the log of observed growth rates using SAS JMP. Important NOM parameters that could explain observed changes in particle growth rates were identified by (1) an associated p-value of $p < 0.05$, signifying a relationship between variables; and (2) the correlation coefficient R^2 which specified the proportion of the variance that was described by a linear relationship (i.e., the quality of the linear fit).

Particle Characterization. Zeta potential of the particle suspensions was quantified by electrophoretic mobility measurements (Malvern Zetasizer) taken 3 h after inducing precipitation. A selection of Zn−S−NOM samples was characterized for morphology and composition by transmission electron microscopy (TEM) coupled with energy dispersive X-ray (EDX) spectroscopy or selected area electron diffraction (SAED). Additional details for sample preparation are provided in the Supporting Information.

RESULTS AND DISCUSSION

Zn−S−NOM precipitation. Upon preparation of the Zn−S−NOM solutions, particles were observed to increase in size over time (Figure 1). These solutions were supersaturated with respect to $ZnS_{(s)}$ (the saturation index log (Q/K_{sp}) was 5.9 for sphalerite, based on equilibrium reactions in Table S2). Thus, the particles formed in the solutions likely consisted of ZnS particles or Zn−S−NOM coprecipitates.[20]

Observed growth rates of particles in the Zn−S−NOM mixtures depended on several factors, including NOM type and concentration (relative to zinc and sulfide), ionic strength, and pH. A subset of the humic substances was capable of stabilizing particles with diameters less than 100 nm for several hours and up to 3 days in our experiments (Figure 1a). Growth of the Zn−S−NOM precipitates tended to be slower with the humic acid fraction when compared to the fulvic acid fraction from the same aquatic source (Figure 1b).

TEM images of the Zn−S−NOM particles (SI Figures S2 and S3) demonstrated aggregates of small electron-dense subunits (<10 nm) that likely consisted of ZnS nanoparticles or clusters. These subunits were surrounded by a material that was less electron-dense (light gray color), which could consist of NOM or an amorphous Zn−S−NOM mixture. SAED results did not demonstrate any distinct diffraction patterns. While some lattice arrangements were observed in the TEM images, the particles were primarily amorphous in structure.

Growth Rates As a Function of Solution Composition. The DLS data were used to understand how growth and aggregation kinetics changed as a function of solution composition and NOM type. Observed rates $(dD/dt)_o$ were calculated from the DLS data (plotted as diameter versus precipitation time) by taking the slope of a linear regression of diameters less than 500 nm. The square of the correlation coefficient (R^2) was greater than 0.8 for most samples. R^2 values were lower (0.5−0.8) for several samples (Suwannee and Ohio River humic acids) that were tracked for more than one day due to slow growth rates. Rates were averaged between 2 or 3 replicate samples in most cases.

The observed growth rates in the ZnS suspensions were strongly dependent on solution composition. Rates increased with increasing ionic strength ($NaNO_3$ electrolyte; Figure 2a), indicating that electrostatic repulsion was one component influencing the change in aggregate size in our experiments. Observed rates also decreased with additional dissolved NOM, sometimes by orders of magnitude and depending on the type of NOM (Figure 2b). Some NOM fractions, such as fulvic acid (Figure 2b) and humic acid (data not shown) from the Suwannee River, decreased growth rates by more than 2 orders of magnitude relative to the NOM-free control.

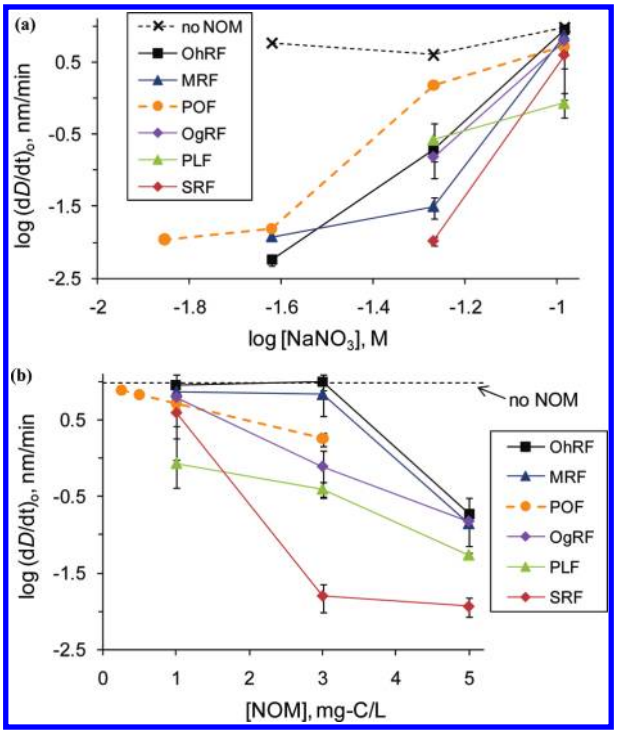

Figure 2. Observed growth rates of Zn−S−NOM particles varied by orders of magnitude depending on water composition variables: (a) $NaNO_3$ background electrolyte (1 mg C/L NOM, 5 μM Zn + S, pH 7.5); (b) NOM concentration (0.1 M $NaNO_3$, 5 μM Zn + S, pH 7.5).

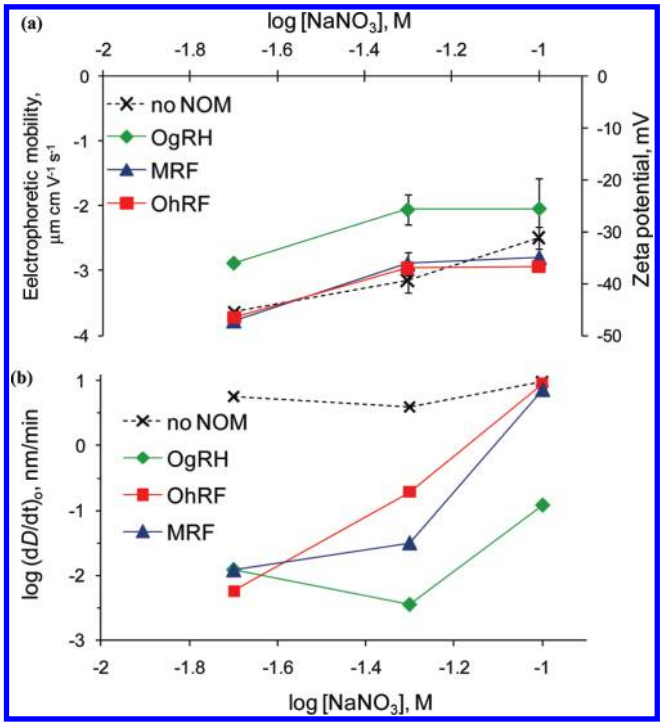

Figure 3. (a) Zeta potential of Zn−S−NOM particles (inferred from electrophoretic mobility) after 3 h of precipitation with 1 mg C/L NOM and 0.02−0.1 M $NaNO_3$. Data points represent the average ±1 SD of triplicate measurements. (b) Observed growth rates quantified for Zn−S−NOM mixtures with 1 mg C/L NOM. All Zn−S−NOM suspensions consisted of 5 μM Zn and 5 μM sulfide in HEPES buffer (pH 7.5).

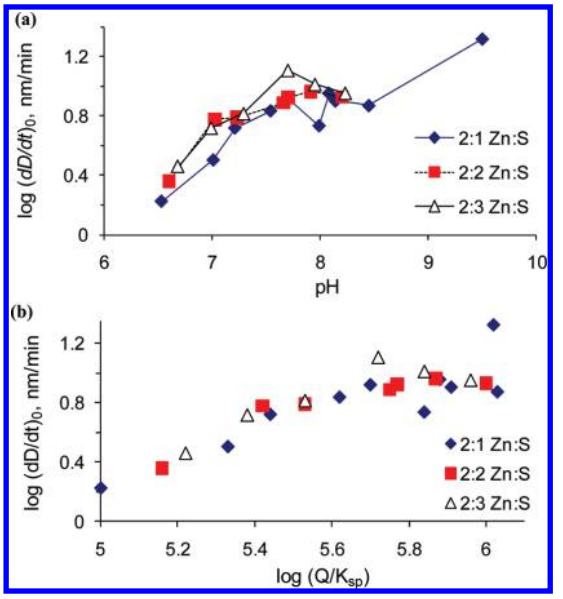

Figure 4. (a) Growth of ZnS particles (no NOM) as a function of pH and varying molar ratios of Zn/S. The samples contained 2 μM $Zn(NO_3)_2$ and 1 to 3 μM Na_2S (4 mM HEPES buffer, 0.01 M $NaNO_3$). (b) Growth data plotted versus the calculated saturation index for sphalerite $ZnS_{(s)}$.

We quantified zeta potential at 3 h of precipitation for a selection of the Zn−S−NOM mixtures: Missouri River fulvic, Ohio River fulvic, and Ogeechee River humic acids (Figure 3a). These NOM isolates reduced observed rates by 1−3 orders of magnitude relative to the NOM-free control (Figure 3b). The results did not demonstrate consistency between zeta potential and observed growth rates. Zeta potentials for the two fulvic acids ranged from −35 mV to −47 mV, values that were similar to the NOM-free control. The Ogeechee River humic samples demonstrated zeta potentials that were less negative (from −23 to −36 mV) even though observed rates were slower than those of the other two NOM isolates (at 10^{-1} M and $10^{-1.3}$ M $NaNO_3$). These data suggest that, while the NOM coatings maintained the net negative charge on particle surfaces, the decrease in growth rates was not simply an electrostatic effect. The adsorbed NOM macromolecules likely caused additional effects, such as steric interactions.[13,14]

ZnS particle growth rates also strongly depended on solution pH (Figure 4). If the observed rates were simply reflecting repulsive forces from surface charge, then an increase in pH would decrease rates (due to net negative charge of surfaces and isoelectric point near pH 7.5 for ZnS particles [11]). Our results, however, showed the opposite. Rates increased by an order of magnitude as pH varied from 6.5 to 9 in solutions containing 2 μM Zn and S (no NOM) (Figure 4a). Modifications to Zn/S molar ratios (from 2:1, 2:2, and 2:3 Zn/S) resulted in little or no change in the observed aggregation rate of particles. Overall, the rates increased with the extent of $ZnS_{(s)}$ supersaturation (Figure 4b), suggesting that observed rates were sensitive to nucleation kinetics and particle concentration. These results highlighted that nucleation and aggregation were occurring simultaneously in our experiments. Therefore, NOM could be influencing observed growth rates by chelating Zn^{2+} and reducing the ZnS saturation index, in addition to imparting electrosteric hindrances for aggregation.

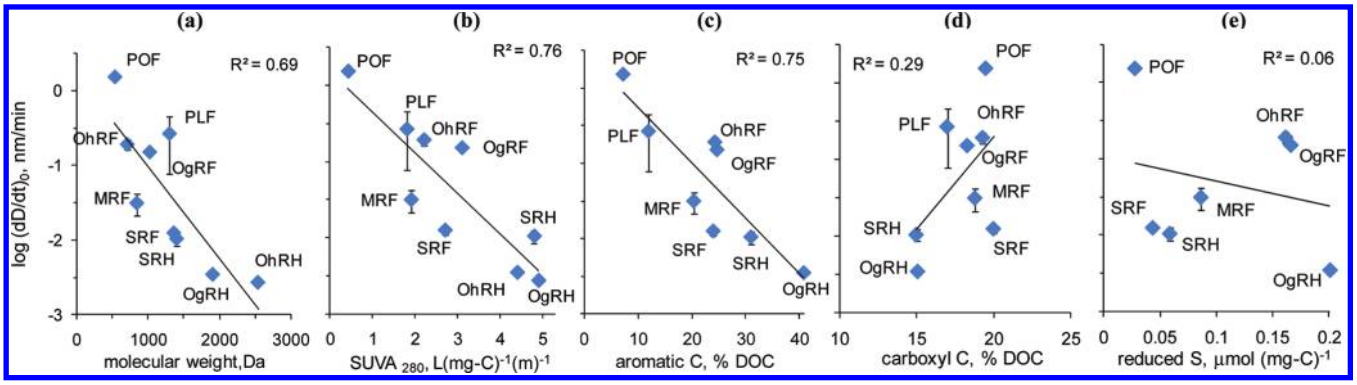

Figure 5. Observed growth rate of Zn−S−NOM particles plotted versus NOM parameters: (a) molecular weight; (b) specific UV absorbance (280 nm); (c) aromatic carbon content; (d) carboxyl carbon content; and (e) reduced sulfur content. Solution composition: 5 μM ZnS, 1 mg C/L NOM, 0.05 M $NaNO_3$, 4 mM HEPES buffer (pH 7.5). Error bars represent ±1 SD of replicate samples (n = 2−3).

Table 2. Parameters for Linear Regressions between Log of Aggregation Rates $(dD/dt)_0$ of Zn−S−NOM Particles and NOM Properties

I = 0.05 M, DOC = 1 mg/L, n = 9					I = 0.1 M, DOC = 3 mg/L, n = 9				
NOM property	m	b	R^2	p	NOM property	m	b	R^2	p
$SUVA_{280}$ (L mg C^{1-} m^{-1})	−0.53	0.18	0.76	0.002*	molecular wt	−0.0014	1.2	0.62	0.01*
aromatic C (% DOC)	−0.073	0.47	0.75	0.003*	$SUVA_{280}$ (L mg C^{1-} m^{-1})	−0.52	0.97	0.52	0.02*
total aliphatic I + II (%DOC)	0.060	−4.3	0.74	0.003*	H (wt %)	1.0	−5.5	0.36	0.10
molecular wt	−0.001	0.22	0.69	0.006*	aromatic C (% DOC)	−0.055	0.86	0.27	0.20
aliphatic I (% DOC)	0.052	−3.3	0.61	0.02*	carboxyl (% DOC)	0.29	−5.6	0.27	0.19
acetal (% DOC)	−0.23	−0.13	0.50	0.03*	carbonyl (% DOC)	−0.24	0.39	0.24	0.22
H (wt %)	0.82	−5.4	0.32	0.07	total aliphatic I + II (%DOC)	0.043	−2.6	0.24	0.22
carbonyl (% DOC)	−0.21	−0.52	0.28	0.17	aliphatic II (% DOC)	0.24	−3.3	0.22	0.24
carboxyl (% DOC)	0.24	−5.5	0.29	0.17	O/C molar ratio	−8.7	3.9	0.22	0.21
aliphatic II (% DOC)	0.12	−2.7	0.09	0.54	O (wt %)	−0.14	4.4	0.19	0.28
O (wt %)	−0.073	1.3	0.08	0.49	aliphatic I (% DOC)	0.033	−1.7	0.15	0.34
reduced S (μmol mg C^{1-})	−3.2	−0.97	0.06	0.51	acetal (% DOC)	−0.13	0.22	0.10	0.43
O/C molar ratio	−3.9	0.63	0.06	0.48	C (wt %)	0.20	−11.5	0.10	0.39
N (wt %)	0.10	−1.6	0.04	0.58	reduced S (μmol mg C^{1-})	1.9	−0.62	0.01	0.82
S (wt %)	0.030	−1.4	0.00	0.85	N (wt %)	0.009	−0.56	0.00	0.98
C (wt %)	−0.00025	−1.4	0.00	0.97	S (wt %)	−0.013	−0.53	0.00	0.83

[a] Regression equation: $\log_{10}$ (growth rate) = m (NOM property) + b. Significant p values ($p < 0.05$) are denoted by *. Aggregation rate $(dD/dt)_0$ units in nm min^{-1}

Correlations with NOM Properties. The NOM isolates used in these experiments represented a diverse array of dissolved humic substances. Differences in composition among the isolates may explain the variation in observed particle growth rates during ZnS precipitation. To better understand the NOM properties with the greatest influence on observed rates, we performed linear regressions between the observed growth rates for the Zn−S−NOM mixtures and specific NOM parameters. R^2 and p values, which were used to assess correlation quality with each NOM parameter, varied depending on the sample electrolyte ($NaNO_3$) and NOM concentrations. In experiments with 1 mg C/L NOM in 0.05 M $NaNO_3$ (a mixture where observed rates decreased by 1−3 orders of magnitude relative to the NOM-free control), the NOM parameters producing the best correlation were $SUVA_{280}$ (R^2 = 0.76, p = 0.002) and aromatic carbon (R^2 = 0.75, p = 0.003) (Figure 5, Table 2). $SUVA_{280}$ is an indicator of aromatic carbon content,[27,30] and aggregation rates decreased as both of these parameters increased (Figure 5). Rates also increased with increasing total aliphatic carbon (R^2 = 0.74, p = 0.003), an expected result since a decrease in aromatic carbon in NOM should lead to an increase in aliphatic carbon.

For mixtures with greater NOM and ionic strength (3 mg C/L NOM in 0.1 M $NaNO_3$), molecular weight was the parameter providing the best correlation with growth rates (R^2 = 0.62, p = 0.01, Table 2). Overall, for the various mixtures tested in this study (DOC 1, 3, and 5 mg C/L; 0.05 or 0.1 M ionic strength), molecular weight and $SUVA_{280}$ were two parameters that consistently ranked in the top four (sorted by R^2 value) for all NOM parameters tested in the correlations (Table 2 and SI Tables S3 and S4).

Parameters that are associated with NOM charge density (carboxyl carbon content, oxygen/carbon ratio) did not demonstrate good correlations with the observed growth rates (Figure 5, Table 2, SI Tables S3 and S4). Moreover, no or weak correlations were observed with the reduced sulfur content and carboxylate carbon content of the NOM (Figure 5). These

functional groups are capable of binding dissolved Zn^{2+}, resulting in decreased saturation index and nucleation rates. These functional groups are also capable of sorbing to the surface of ZnS clusters and nanoparticles. However, in our experiments, equilibration time between Zn and NOM (less than 5 min) was probably too short to allow for Zn binding by the strong, low abundance ligands in NOM.[31]

While overall growth rates of Zn−S−NOM particles were influenced by repulsive forces for aggregation caused by the net negative surface charge, the variations between the NOM fractions were explained mostly by properties that influenced steric effects. For example, an increase in molecular weight would presumably lead to thicker adsorbed layers of NOM on the ZnS particles, particularly if NOM forms loop and tail structures then extend away from particle surfaces.[12,13,19] The correlations with $SUVA_{280}$ are consistent in that high molecular weight NOM tends to have more aromatic carbon over aliphatic carbon moieties.[27] Furthermore, parameters for specific metal binding capacity (carboxylate and reduced sulfur) were not important for observed differences between the NOM. In our experiments, the Zn and sulfide concentrations exceeded the reduced-S content of the NOM by 1 or 2 orders of magnitude. As a result, thiol complexation of dissolved Zn^{2+} was not a factor for growth rates. Even the weaker, more abundant ligand group (carboxylates) did not appear to correlate with observed rates. These results suggested that Zn^{2+} complexation was not a prominent factor for the Zn, S, and NOM concentrations utilized in this study; however, for ZnS nanoparticles, a fraction of all Zn atoms are at the surface. Thus, we cannot rule out the possibility that a subset of the oxygen- and sulfur-containing functional groups within the NOM macromolecule (i.e., those associated with aromatic carbon) were specifically binding to surface Zn atoms on nanoparticle surfaces.

Environmental Significance. Our results highlight the important molecular components of NOM that may be responsible for controlling the precipitation and aggregation of ZnS nanoparticles. The sorbed NOM layer induced electrosteric repulsive forces that slowed aggregates rates. While all of the NOM fractions induced net negative surface potential on the Zn−S−NOM particles, macromolecular properties that contribute to electrosteric effects seemed to differentiate the NOM isolates. The molecular size and structure of the NOM was likely influencing the thickness of the adsorbed layer, and consequently, particle−particle interactions during aggregation. Therefore, stabilization and persistence of ZnS nanoparticles would be expected not only in organic-rich settings, but also in waters containing dissolved NOM of high molecular weight or aromatic content.

NOM is also capable of complexing Zn (either dissolved ions or atoms on the ZnS surface). However, our results indicated that the density of ligand binding groups (reduced sulfur and carboxylate) was not a factor for growth rates. Alternatively, preferential metal binding could have occurred with ligand groups associated with aromatic carbon. However, this work did not differentiate between functional groups associated with aromatic or aliphatic carbon.

Overall, the results of this study provide insight toward the types of environments that allow for ZnS nanoparticles to persist in the natural environment. This information also provides clues to the behavior of manufactured nanoparticles released in aquatic settings with different types of dissolved organic carbon. The application of DLS in this study limited the interpretation of this research to aggregation processes during ZnS precipitation. Further studies could investigate how NOM alters the early stages of precipitation including polynuclear cluster formation.

■ ASSOCIATED CONTENT

Supporting Information. Tables of NOM properties and correlation parameters. Figures of Zn−S−NOM precipitation with different pH buffers, TEM images of Zn−S−NOM aggregates, and DLS data for Zn−S−NOM mixtures. This information is available free of charge via the Internet at http://pubs.acs.org/ .

■ AUTHOR INFORMATION

Corresponding Author
*Phone: (919) 660-5109; e-mail: hsukim@duke.edu.

Present Addresses
§Department of Geology, Baylor University, One Bear Place #97354, Waco, TX 76798.

■ ACKNOWLEDGMENT

We thank J. Nason at Oregon State University and C. Gerbig at CU-Boulder for their valuable comments to the manuscript. This research was support by the Center for Environmental Implications of Nanotechnology, funded by the National Science Foundation and the U.S. Environmental Protection Agency. TEM images were acquired with the help of R. Garcia at the NC State Analytical Instrumentation Facility and M. Gignac at the Duke University Shared Materials Instrumentation Facility. The use of brand names in this report is for identification purposes only and does not imply endorsement by the U.S. Geological Survey.

■ REFERENCES

(1) DiToro, D. M.; Mahony, J. D.; Hansen, D. J.; Scott, K. J.; Carlson, A. R.; Ankley, G. T. Acid volatile sulfide predicts the acute toxicity of cadmium and nickel in sediments. *Environ. Sci. Technol.* **1992**, *26* (1), 96–101.

(2) Liu, J.; Aruguete, D. M.; Murayama, M.; Hochella, M. F. Influence of size and aggregation on the reactivity of an environmentally and industrially relevant nanomaterial (PbS). *Environ. Sci. Technol.* **2009**, *43* (21), 8178–8183.

(3) Weber, F.-A.; Voegelin, A.; Kaegi, R.; Kretzschmar, R. Contaminant mobilization by metallic copper and metal sulphide colloids in flooded soil. *Nat. Geosci.* **2009**, *2* (4), 267–271.

(4) Hochella, M. F.; Moore, J. N.; Putnis, C. V.; Putnis, A.; Kasama, T.; Eberl, D. D. Direct observation of heavy metal-mineral association from the Clark Fork River Superfund Complex: Implications for metal transport and bioavailability. *Geochim. Cosmochim. Acta* **2005**, *69* (7), 1651–1663.

(5) Labrenz, M.; Druschel, G. K.; Thomsan-Ebert, T.; Gilbert, B.; Welch, S. A.; Kemner, K. M.; Logan, G. A.; Summons, R. E.; De Stasio, G.; Bond, P. L.; Lai, B.; Kelly, S. D.; Banfield, J. F. Formation of sphalerite (ZnS) deposits in natural biofilms of sulfate-reducing bacteria. *Science* **2000**, *290*, 1744–1747.

(6) Moreau, J. W.; Weber, P. K.; Martin, M. C.; Gilbert, B.; Hutcheon, I. D.; Banfield, J. F. Extracellular proteins limit the dispersal of biogenic nanoparticles. *Science* **2007**, *316* (5831), 1600–1603.

(7) Rozan, T. F.; Lassman, M. E.; Ridge, D. P.; Luther, G. W. Evidence for iron, copper and zinc complexation as multinuclear sulphide clusters in oxic rivers. *Nature* **2000**, *406* (24), 879–882.

(8) Kim, B.; Park, C.-S.; Murayama, M.; Hochella, M. F., Jr. Nanoparticles in biosolid products as revealed by electron microscopy.

Geochim. Cosmochim. Acta **2010**, *74* (12, Supplement 1), A487–A552.

(9) Bebie, J.; Schoonen, M. A. A.; Fuhrmann, M.; Strongin, D. R. Surface charge development on transition metal sulfides: An electrokinetic study. *Geochim. Cosmochim. Acta* **1998**, *62* (4), 633–642.

(10) Horzempa, L. M.; Helz, G. R. Controls on the stability of sulfide sols - colloidal covellite as an example. *Geochim. Cosmochim. Acta* **1979**, *43* (10), 1645–1650.

(11) Gondikas, A. P.; Jang, E. K.; Hsu-Kim, H. Influence of amino acids cysteine and serine on aggregation kinetics of zinc and mercury sulfide colloids. *J. Colloid Interface Sci.* **2010**, *347* (2), 167–171.

(12) Au, K. K.; Penisson, A. C.; Yang, S. L.; O'Melia, C. R. Natural organic matter at oxide/water interfaces: Complexation and conformation. *Geochim. Cosmochim. Acta* **1999**, *63* (19−20), 2903–2917.

(13) Tiller, C. L.; O'Melia, C. R. Natural organic matter and colloidal stability: Models and measurements. *Colloids Surf., A* **1993**, *73*, 89–102.

(14) Liang, L.; Morgan, J. J. Chemical aspects of iron-oxide coagulation in water - laboratory studies and implications for natural systems. *Aquat. Sci.* **1990**, *52* (1), 32–55.

(15) Ravichandran, M.; Aiken, G. R.; Reddy, M. M.; Ryan, J. N. Enhanced dissolution of cinnabar (mercury sulfide) by dissolved organic matter isolated from the Florida Everglades. *Environ. Sci. Technol.* **1998**, *32*, 3305–3311.

(16) Waples, J. S.; Nagy, K. L.; Aiken, G. R.; Ryan, J. N. Dissolution of cinnabar (HgS) in the presence of natural organic matter. *Geochim. Cosmochim. Acta* **2005**, *69* (6), 1575–1588.

(17) Ravichandran, M.; Aiken, G. R.; Ryan, J. N.; Reddy, M. M. Inhibition of precipitation and aggregation of metacinnabar (mercuric sulfide) by dissolved organic matter isolated from the Florida Everglades. *Environ. Sci. Technol.* **1999**, *33* (9), 1418–1423.

(18) Deonarine, A.; Hsu-Kim, H. Precipitation of mercuric sulfide nanoparticles in NOM-containing water: Implications for the natural environment. *Environ. Sci. Technol.* **2009**, *43* (7), 2368–2373.

(19) Phenrat, T.; Song, J. E.; Cisneros, C. M.; Schoenfelder, D. P.; Tilton, R. D.; Lowry, G. V. Estimating attachment of nano- and submicrometer-particles coated with organic macromolecules in porous media: Development of an empirical model. *Environ. Sci. Technol.* **2010**, *44* (12), 4531–4538.

(20) Lau, B.; Hsu-Kim, H. Precipitation and growth of Zn-sulfide nanoparticles in the presence of thiol-containing natural organic ligands. *Environ. Sci. Technol.* **2008**, *42* (19), 7236–7241.

(21) Xia, K.; Weesner, F.; Bleam, W. F.; Bloom, P. R.; Skyllberg, U. L.; Helmke, P. A. XANES studies of oxidation states of sulfur in aquatic and soil humic substances. *Soil Sci. Soc. Am. J.* **1998**, *62* (5), 1240–1246.

(22) Al-Farawati, R.; van den Berg, C. M. G. Thiols in coastal waters of the western North Sea and English Channel. *Environ. Sci. Technol.* **2001**, *35* (10), 1902–1911.

(23) Vairavamurthy, A.; Mopper, K. Field methods for determination of traces of thiols in natural waters. *Anal. Chim. Acta* **1990**, *236*, 363–370.

(24) Zhang, J.; Wang, F. Thiols in wetland interstitial waters and their role in mercury and methylmercury speciation. *Limnol. Oceanogr.* **2004**, *49* (6), 2276–2286.

(25) Mopper, K.; Taylor, B. F., Biogeochemical cycling of sulfur; thiols in coastal marine sediments. In *ACS Symposium Series 305; Organic Marine Geochemistry*; Sohn, M. L., Ed.; American Chemical Society: Washington, DC, 1986; pp 324−339.

(26) Thurman, E. M.; Malcolm, R. L. Preparative isolation of aquatic humic substances. *Environ. Sci. Technol.* **1981**, *15* (4), 463–466.

(27) Chin, Y. P.; Aiken, G.; Oloughlin, E. Molecular weight, polydispersity, and spectroscopic properties of aquatic humic substances. *Environ. Sci. Technol.* **1994**, *28* (11), 1853–1858.

(28) Cabaniss, S. E.; Zhou, Q.; Maurice, P. A.; Chin, Y. P.; Aiken, G. R. A log-normal distribution model for the molecular weight of aquatic fulvic acids. *Environ. Sci. Technol.* **2000**, *34* (6), 1103–1109.

(29) Vairavamurthy, M. A.; Maletic, D.; Wang, S. K.; Manowitz, B.; Eglinton, T.; Lyons, T. Characterization of sulfur-containing functional groups in sedimentary humic substances by X-ray absorption near-edge structure spectroscopy. *Energy Fuels* **1997**, *11* (3), 546–553.

(30) Weishaar, J. L.; Aiken, G. R.; Bergamaschi, B. A.; Fram, M. S.; Fujii, R.; Mopper, K. Evaluation of specific ultraviolet absorbance as an indicator of the chemical composition and reactivity of dissolved organic carbon. *Environ. Sci. Technol.* **2003**, *37* (20), 4702–4708.

(31) Miller, C. L.; Southworth, G.; Brooks, S.; Liang, L.; Gu, B. Kinetic Controls on the Complexation between Mercury and Dissolved Organic Matter in a Contaminated Environment. *Environ. Sci. Technol.* **2009**, *43* (22), 8548–8553.